EFDA–JET–PR(09)42

M. Romanelli, A. Zocco, F. Crisanti
and JET EFDA contributors

Fast Ion Stabilization of the Ion Temperature Gradient Driven Modes in the Joint European Torus Hybrid-Scenario Plasmas: A Trigger Mechanism for Internal Transport Barrier Formation

Fast Ion Stabilization of the Ion Temperature Gradient Driven Modes in the Joint European Torus Hybrid-Scenario Plasmas: A Trigger Mechanism for Internal Transport Barrier Formation

M. Romanelli[1], A. Zocco[1,2,3*], F. Crisanti[4] and JET EFDA contributors*

JET-EFDA, Culham Science Centre, OX14 3DB, Abingdon, UK

[1]EURATOM-CCFE Fusion Association, Culham Science Centre, OX14 3DB, Abingdon, OXON, UK
[2]Politecnico di Torino, C.so Duca degli Abruzzi 24, 10129 Torino, Italy
[3]Wolfgang Pauli Institute, Univ. Of Vienna, A-1090 Vienna, Austria
** See annex of F. Romanelli et al, "Overview of JET Results",*
(Proc. 22 [nd] IAEA Fusion Energy Conference, Geneva, Switzerland (2008)).

Preprint of Paper to be submitted for publication in
Plasma Physics and Controlled Fusion

ABSTRACT.

Understanding and modelling turbulent transport in thermonuclear fusion plasmas is crucial for designing and optimizing the operational scenarios of future fusion reactors. In this context, plasmas exhibiting state transitions, such as the formation of an internal transport barrier (ITB), are particularly interesting since they can shine light on transport physics and offer the opportunity to test different turbulence suppression models. In this paper we focus on the modelling of ITB formation in the Joint European Torus (JET) [1] hybrid-scenario plasmas, where, due to the monotonic safety factor profile, magnetic shear stabilization cannot be invoked to explain the transition. The turbulence suppression mechanism investigated here relay on the increase of the plasma pressure gradient in the presence of a minority of energetic ions. Micro-stability analysis of the ion temperature gradient driven modes (ITG) in the presence of a fast-hydrogen minority show that energetic ions accelerated by the ion cyclotron resonance heating (ICRH) system (hydrogen, $n_{H,fast}/n_{D,thermal}$ *up to 10%*, $T_{H,fast}/T_{D,thermal}$ *up to 30*) can increase the pressure-gradient enough to stabilise the ITG modes driven by the gradient of the thermal ions (deuterium). Numerical analysis shows that, by increasing the temperature of the energetic ions, electrostatic ITG modes are gradually replaced by nearly-electrostatic modes with tearing parity at progressively longer wavelengths. The growth rate of the micro tearing modes is found to be lower than that of the ITG modes and comparable to the local $E\times B$-velocity shearing-rate. The above mechanism is proposed as a possible trigger for the formation of internal transport barriers in this type of discharges.

1. INTRODUCTION

Advanced plasma scenarios have been developed at the Joint European Torus (JET) [1] with the aim of providing higher normalized plasma pressure, β_N, and/or longer pulse duration

compared with the ELMy (Edge Localised Mode) H-mode envisaged for the reference inductive operation of ITER [2]. These scenarios are in general referred to as "Advanced Tokamak scenarios", and are divided in two types: the "steady-state advanced scenario" and the "hybrid" scenario. Good performances have been achieved in both types of scenarios in several Tokamaks (JET, Doublet III-D (DIII-D) [3], ASDEX Upgrade (AUG) [4], JAERI Tokamak Upgrade (JT-60U) [5]) and a quasi steady-state high value of β_N has been obtained [6,7,8]. The "steady-state" approach relies on the development of a region of improved thermal insulation in the core, called an Internal Transport Barrier (ITB) [6,9], to provide high fusion performance and large self-generated bootstrap current necessary for efficient steady-state operations. The minimum value of q (safety factor) achieved in such discharges is generally in the range *1.5 - 2.0*, whilst the magnetic shear can be negative or close to zero. The formation of the ITB in the above type of plasmas is well correlated to the reversal of the magnetic shear and the radial position of the barrier to the radial position of the minimum q. A different approach, aimed at producing high $H\beta_N$ plasmas [2], is taken in the "hybrid" scenario [10], and relies on keeping the central safety factor just above unity in a large region of monotonic, positive, low magnetic shear. This scenario, sometimes also called "improved H-mode" [11], is often characterized by good confinement at the plasma edge [12] and the absence of the sawtooth trigger for large Neoclassical Tearing Modes (NTMs) [13]. Although improved confinement in the hybrid scenario is achieved without transport barriers, the possibility to further improve the confinement by forming an ITB was established in JET [14] during a campaign dedicated to similarity experiments with AUG. In this paper we will not attempt to explain the improvement of confinement observed in the standard hybrid scenario but we will focus on studying the trigger for the formation of the internal transport barrier in the absence of reversed magnetic shear by investigating the stability of ITG turbulence in the presence of ion-cyclotron-resonance heating (ICRH) produced fast-ion minority. As discussed

in section IV, we find in the numerical analysis that by increasing locally the temperature of the energetic-ion minority, electrostatic ITG modes are gradually replaced by nearly-electrostatic modes with tearing parity at progressively longer wavelengths. The growth rate of the micro tearing modes is found to be lower than that of the ITG modes and comparable to the local $E\times B$-velocity shearing-rate. The paper is organized as follows: in section II we describe in details a JET hybrid-scenario discharge (#59137) which will be used as reference for the micro stability analysis, in section III we report on the ITG linear-stability analysis in the presence of an increasingly-energetic ion-minority, in section IV we discuss the properties of the unstable modes, the appearance of the micro tearing instability and the scaling of its growth rate with the energetic-ion pressure-gradient, and finally conclusions are in section V.

2. CHARACTERIZATION OF JET HYBRID SCENARIO PULSE NO: 59137

A large data base of hybrid discharges is presently available at the Joint European Torus and the scenario is still subject of developments. In Fig. 1 it is shown the central density and temperature of a set of hybrid discharges with same input power (within 5%). One of the best examples of high core confinement is pulse #59137 (toroidal magnetic field $B_T = 2.55\ T$, plasma current $I_p = 2.2\ MA$, ion normalized Larmor radius $\rho^* \sim 5.5\times10^{-3}$, neutral beam injected power $P_{NBI} = 13.4\ MW$, ion cyclotron resonance heating on hydrogen minority, frequency $42\ MHz$, resonance $R=2.77\ m$, injected power $P_{ICRH} = 2.5\ MW$, normalized collision frequency $\nu^*_e \sim 0.05$ where the normalization is the standard one adopted for ITER studies [2]). This discharge has been obtained with the JET hybrid-scenario operational scheme shown in Fig. 2, that led to a large central region in which $1 < q < 1.5$, Fig. 3, as confirmed by the MSE (Motional Stark Effect) measurements, by the Faraday Rotation measurements and by the absence of sawtooth activity. With reference to Fig. 2, the central ion and electron temperatures reach 17 keV and 8 keV respectively during the current plateau.

These are temperatures above those of similar discharges with identical heating power. In this particular discharge, the reason of the higher ion and electron temperature lays in the development of a wide region around *r/a=0.4, R=3.4 m* (*Δr ~ 0.2 m* between *r/a=0.33, R=3.3 m and r/a=0.5, R=3.5 m*) characterized by steep electron and ion temperature gradients and large normalized inverse gradient scale-lengths up to $R/L_{Ti} \sim 14$, $R/L_{Te} \sim 11$, although at different radial positions (Fig. 4 discussed later). The above gradients are the signature of an internal transport barrier which forms at *t=8.7 s* and radial position *R=3.4 m, r/a=0.4* for the ions and *R=3.3 m, r/a=0.33* for the electrons. The barrier appears in the ion temperature profile in coincidence with a transition of the coupled ICRH power. As discussed in [15], JET ITBs are characterized by values of the normalized Larmor-radius $\rho^*_{Ti,e} > 1.4\times10^{-2}$, where $\rho^*_{T_{i,e}} = \rho_s \nabla T_{e,i} / T_{e,i} = \rho_s / L_{T_{e,i}} = \rho^* R / L_{T_{e,i}}$. The time evolution of the radial profiles of electrons and ions normalized Larmor-radius, ρ^*_{Te}, and ρ^*_{Ti} respectively is plotted in Fig. 4. It is evident that the region of $\rho^*_{Ti} > 1.4\times10^{-2}$ is radially extended, whereas the electron barrier region is narrower and closer to the plasma centre. Here it is important to mention that the ion temperature profile (Fig. 5) is measured at a lower radial resolution (*Δr=8 cm*) as compared to the electron temperature. The steep gradients last for around *5 s*, only limited by the duration of the NBI. In Fig. 5 we report the radial profiles of the electron and ion temperatures (from the Electron Cyclotron Emission and from the Charge-Exchange), of the electron density (from the Thomson scattering) and of the toroidal rotation (from the Charge-Exchange), at four different times. The profiles of Fig. 5 show the transition phase to the enhanced central confinement and the highest performance, in particular the ion temperature profile at *t=10 s* (dotted line) shows the effect of the barrier inside *R=3.5, r/a=0.5*. During the initial part of the heating phase, the edge temperatures are $T_i \approx T_e \sim 2$ *keV*, and in correspondence of a small step-up of the NBI power (Fig. 2, *t=10.5 s*) they increase of *2 keV* and *1 keV*, respectively, Fig. 5; at the same time, the edge densities decrease (from

$\sim 2.8\times10^{19}\,m^{-3}$ to $\sim 1.3\times10^{19}\,m^{-3}$) providing a slowly varying edge pressure. A decrease of the central density is also observed (from $\sim 4.4\times10^{19}\,m^{-3}$ to $\sim 3.2\times10^{19}\,m^{-3}$), while the density profile remains moderately peaked. Although the additional heating power is well above the usual H-mode threshold, and above the power normally required to access type I ELMs, for a long period the discharge exhibits only a weak ELM activity characterized by tiny type-I ELMs. The global performance is comparable to, or slightly better than, that of similar hybrid discharges with large type-I ELMs ($\beta_N \sim 2$, $H_{89} \sim 2.2$ and $\beta_N H_{89}/q_{95}^2 \sim 0.3$). Another characteristic of pulse #59137 is that the plasma energy associated with the pedestal is $W_{ped} \sim 37\%$, comparable with the energy of standard H-mode. It is also worth observing that the energy within the steep gradient region ($r/a<0.3$) is $W_{core} \sim 23\%$, in spite of the low density and of the small plasma volume involved. The toroidal rotation in #59137 is $\omega_T \sim 1.2\times10^5\,rad/s$ with a quite moderate and constant shear. The $E\times B$ shearing rate is large ($\omega_{E\times B} \sim 1.5\times10^5\,s^{-1}$), when calculated assuming neoclassical poloidal rotation (although this assumption has recently been called into question [16]).

The equilibrium, sources, and plasma profiles of #59137 required for the micro stability analysis of section III have been validated by running a detailed interpretative transport analysis with the JETTO transport code [17]. The energy and density profiles of the NBI fast deuterium and of the ICRH accelerated hydrogen ions have been calculated with the PENCIL code [1] and the PION code (discussed later) respectively. It is noticeable that the transport barrier observed in #59137 is not present in similar discharges in the database which have identical operational parameters but higher density. We have compared the heat sources and effective conductivities of #59137 ($n_e=2\times10^{19}\,m^{-3}$) with two such discharges in the database (#60933, #62459) having increasingly higher line average density ($n_e= 3\times10^{19}\,m^{-3}$ and $n_e= 5.5\times10^{19}m^{-3}$ respectively). Concerning the heat sources, the total coupled power to the electrons and to the ions is similar for the three discharges. The fraction of power absorbed by

the ions (8 ÷ 10 MW) is larger than the one absorbed by the electrons (4.5 ÷ 6.5 MW). The total power deposition profile has approximately the same peaking factor; in the lower density discharge the power is coupled at a larger radius than in the other two (*r/a ~ 0.35*, instead of *r/a ~ 0.2*) this has to be attributed to the different temperature and density profiles rather than an effect of the low density. The ion and electron thermal conductivities, $\chi_{i,}$ χ_e show a decrease over the entire central region consistent with the presence of the transport barrier inside *r/a=0.5*. In Fig. 6 the time traces of the ion thermal conductivity of the three discharges are plotted at two (normalized) radial positions: *r/a= 0.3* and *r/a = 0.7*. At one third of the minor radius the ion thermal conductivity is smaller in the discharge with the lowest central plasma density and with the largest central ion and electron temperatures; increasing the density also increases χ_i. The opposite behaviour is observed in the external region, 70% of the minor radius, where the conductivity decreases along with the density, indicating a better confinement in the discharges with higher density. Related to the different electron densities there is a different contribution of the non-thermal particles to the total energy and density content. In pulse #59137 around 40% of the total energy is in the fast-ion population. The main contribution to the total fast-ion density comes from the fast-deuterium produced by charge exchange of 80 keV beam neutrals. However, in the transport barrier region, the fast-hydrogen density is about 4% of the total line averaged electron density and exceeds by around a factor two the density of the beam deuterium-ions. In Fig. 7 and Fig. 8 are shown respectively the temperature profile and the density profile of the accelerated hydrogen-ions, evaluated using the code PION [18] and the measured diamagnetic energy with the volume integral of the temperature and density. The contribution of the fast ions to the total energy decreases to around 30% for the intermediate-density pulse (#60933) and becomes just ~ 10% for the discharge with the highest density. The presence of the largest fast-ion population in the discharge that develops the transport barrier, suggests that fast-ion may play a role in the

reduction of turbulent transport and trigger the barrier formation, as already shown in [19] for ASDEX Upgrade. The improvement of confinement in the scenario reported in [19] has been attributed to dilution brought about by the fast ions. In the next section we explore a different stabilizing mechanism related to fast-hydrogen pressure gradient. The fast-hydrogen density (Fig. 8) peaks inside the transport barrier and has a steep gradient in the region $0.4<r/a<0.5$ which results in a large contribution of the fast hydrogen to the local pressure gradient. The local change of β and pressure-gradient brought about by the fast-hydrogen modifies the spectrum of the linearly unstable modes (marginal stability thresholds [20]) and can be an important stabilizing mechanism in those plasmas where dilution is not very large (in the case studied ($n_{H+}n_{D,fast}$)/$n_{D,thermal}$~0.13). Electromagnetic micro stability analysis of pulse #59137 at a time around the formation of the barrier, section IV, shows that the temperature gradient modes driven by the deuterium are stabilized in the presence of a fast hydrogen minority at a temperature and density close to those found in the experiment. A much higher hydrogen temperature is required to stabilize the modes in the other two higher density discharges.

3. FAST ION STABILIZATION OF ITG MODES IN JET PULSE NO: 59137

Previous analyses [20,21] have shown that, when β effects are non negligible, micro instabilities driven by the gradient of the ion temperature (ITG) acquire an electromagnetic polarization and are linearly stabilized at increasing values of the α parameter ($\alpha = \beta' q^2 R$ where β' is proportional to the pressure gradient). This α-stabilization continues until a critical value (threshold) is reached above which other branches become unstable. The latter modes have nearly Shear-Alfvén polarization and are generically referred to as either Alfvénic ITGs (AITG) or Kinetic Ballooning Modes (KBM). A rigorous distinction between AITG and KBM can be made based on the sign of the ideal MHD δW for the given pressure gradient: $\delta W>0$ for AITG and $\delta W<0$ for KBM [21,22,23]. The presence of a fast ion minority

in a localized region of the plasma does not contribute significantly to the global pressure of the entire plasma column (the edge β is generally determined solely by the pressure of the thermal species); however it can significantly increase the local value of β and its gradient, therefore changing the polarization of the instabilities driven by the thermal-ion temperature-gradient from electrostatic to electromagnetic. By adding the energetic ion contribution to the plasma pressure, it might be possible to locally reach an optimal value of α (just below the threshold of the Alfvénic modes) for which the "electrostatic" ITGs are stable and the Alfvénic modes are still quiescent. This would allow the plasma to develop ion temperature gradients with inverse scale-lengths well above the threshold for unstable electrostatic ITG [24] and trigger the formation of an ion transport barrier. In order to assess whether the fast ions accelerated in JET discharge #59137 can locally stabilize the ITG turbulence through the mechanism described above, we have analyzed the plasma stability at *t=10 s*, i.e. about 1 s after the formation of the ITB, accounting for an increasingly hot ion minority. As discussed in section II, the most abundant energetic species in the region inside the transport barrier is hydrogen accelerated by the ICRH system. The contribution of the hydrogen to the local β (at the radial position where the hydrogen density is maximum) is at least a factor four larger then that of the fast deuterium from the neutral beams. As shown in Fig. 8 the gradient of the hydrogen density is very steep at the location of the transport barrier and will contribute significantly to increase the thermal α whereas the pressure gradient of the energetic deuterium is of the same order of that of the thermal deuterium. For the reason above in the present analysis we have considered only the hydrogen species as fast ion minority and accounted for the contribution of the fast-deuterium as a correction to the thermal β. The linear growth rate of the ITG modes have been calculated at *r/a=0.5*, at the foot of the ion transport barrier, using the gyrokinetic code GS2 [25]. The code has been run in its linear version including: electron dynamics (non adiabatic electrons) an optimized Lorentz collision

operator, which has also been validated in other codes [26] and full electromagnetic solution (parallel and perpendicular magnetic fluctuations have been included). MHD analysis of pulse #59137 [27] shows that the energetic particles are not driving macroscopic modes such as large fishbones therefore here we will focus on the effect of the high temperature minority on the stability of the turbulence. In the microstability analyses we have included the hydrogen minority as a Maxwellian species. This description does not reflect totally the experimental conditions, where the fast hydrogen-ions are not isotropic and their distribution would be better described by a "slowing down" distribution function. However previous works [19,28] have shown that the Maxwellian model adequately reproduces the scaling of the linear growth rate with the plasma pressure. The local density and temperature gradients of the hydrogen minority as calculated using PION, are affected by large uncertainties; we are therefore free, within the experimental error bars, to assume values for the gradients that simplify the analysis. In order to filter out possible instabilities driven by the temperature-gradient of the H minority we have set it to zero. Furthermore to simplify the plasma neutrality condition, the density gradient of the hydrogen and the deuterium have been taken equal; the latter assumption is also made in PION for the thermal hydrogen, however the gradient of the accelerated hydrogen is found to be larger in the experiment, Fig. 8. The magnetic equilibrium adopted is a local s-α equilibrium. We have not included trapped particle driven modes, therefore a more detailed characterization of the plasma triangularity and ellipticity is not necessary. The value of the equilibrium α-parameter has been calculated including the pressure gradients of all thermal and energetic (fast) species:

$$\alpha = \beta' q^2 R \rightarrow \beta' = \alpha / \left(q^2 R\right) \propto p' = \sum_l \nabla p_l + \frac{n_{fast} T_{fast}}{L_{n,\,fast}}$$

where the summation is over all the thermal species *l*, $p=nT$ is the pressure, *q* is winding index number (safety factor), $L_{n,fast} = n_{fast} / \nabla n_{fast}$ is the inverse density-gradient scale length of the fast minority (hydrogen) and *R* is the plasma major radius (*R =3.0 m*). The values of gradients and densities used in the micro stability analysis have been extracted from the results of the JETTO transport analysis of pulse #59137 at *t=10 s* and *r/a=0.5*, and are summarized in Table I. The other plasma parameters used in the analysis are: magnetic shear *s=0.64, q=1.62,* $\beta_{170KeV}=0.013$, $\beta_{5KeV}=0.008$, where the subscripts of β refer to different temperatures of the hydrogen minority. The hydrogen temperature has been varied between 5 Kev (temperature of the thermal deuterium) and 800 KeV, keeping its density-gradient constant. Here it is worth noticing that the value of $R\nabla n_H / n_H$ used in the analysis (see Table I) is such that a small change in the hydrogen temperature produces a larger change in α. This is better illustrated in figure 9 where it can be seen that by varying the temperature of the minority within the same range a wider range of α can be scanned at $L_{n,fast} / R$ around 1 and below. The spectrum of the unstable modes for the plasma parameters of Table I has been calculated with a hydrogen temperature of 5 keV (Fig 10, $\alpha=0.19$). In this discharge the inverse scale length of the ion temperature gradient (Table I) is well above the JET linear threshold for the ITG [24]. As expected the unstable modes are found to be dominantly electrostatic with ITG parity (see section IV) and the most unstable mode occurs around $k_\perp \rho_i = 0.6$. By increasing the hydrogen temperature above 100 keV, α reaches values above 0.3 and, as shown for example in [21], the instabilities become electromagnetic. The growth rate of the unstable modes decreases as α increases (by increasing the temperature of the hydrogen minority) and for the value of the gradients of Table I the growth rates become comparable to the ω_{ExB} shearing rate at an hydrogen temperature around 170 keV (Fig. 10, α=0.38), in agreement with the experimental hydrogen temperature calculated by PION

for this discharge at *r/a=0.5*, (Fig. 7). As shown in section IV, by increasing α part of the most unstable modes are found to have tearing parity. We highlight here that the mechanism of α-stabilization illustrated above is not the same mechanism discussed in [29] where only electrostatic modes were considered. Indeed by increasing the temperature of the hydrogen in the electrostatic limit we find the same α-stabilization discussed in [29]. This is entirely a geometric effect due to change in the local equilibrium magnetic field (parameterized through α), hence in the ion and electron vertical drift frequency. Figure 11 shows the result of the same hydrogen-temperature scan discussed above but this time in the electrostatic limit (eliminating the magnetic field fluctuations), carried out for one of the most unstable modes and for two different values of the hydrogen normalized density gradient around the values of Table I. The growth rate of the mode decreases with increasing hydrogen temperature, and eventually is fully stabilized above a threshold value which depends on the density gradient of the energetic species, for $R/L_{n,\,fast}=3$ in Fig. 11 the stabilization occurs for $T_{fast}=160$,α=1.38, where $T_{fast}=T_H/T_D$ is the hydrogen temperature normalized to the deuterium temperature. We see here that the temperature of the hydrogen at which the growth rate of the electrostatic ITG is comparable to the ω_{ExB} shearing rate is around a factor five higher than in the electromagnetic analysis. As already pointed out, a small increase of the hydrogen temperature when the density gradient is steep brings about a large increase of α hence full stabilization of the electrostatic modes can be achieved at lower temperatures, however the large values of α imply that the modes have electromagnetic character and the full electromagnetic problem needs to be solved. The influence of the magnetic shear is shown in Fig. 12 where the stability analysis of Fig. 11 has been repeated for three different values of *s*. We find that at lower magnetic shear the threshold temperature for the ITG stabilization is lower, although the variation is not very strong. In contrast for higher magnetic shear we find that stabilization occurs at much higher temperatures. At low values of α the dependence of

the growth rate of the electromagnetic modes on the magnetic shear and on the normalized hydrogen gradient is the same as that of the electrostatic modes, as shown in e.g. [20]. In the next section we will discuss the structure of the electromagnetic modes and the scaling of their growth rate with α above the values presented in Fig. 10.

4. STRUCTURE OF THE ELECTROMAGNETIC MODES AND SCALING OF THEIR LINEAR GROWTH RATE WITH THE HYDROGEN TEMPERATURE

In this section we discuss the structure and properties of the electromagnetic modes shown in Fig. 10, of section III. In order to address the mode structure we need first to introduce the eigenvalue equations for the full electromagnetic problem

$$\begin{aligned} L_\phi \delta\phi &= \lambda_\phi \delta\phi \\ L_A \delta A_\parallel &= \lambda_A \delta A_\parallel \\ L_B \delta B_\parallel &= \lambda_B \delta B_\parallel \end{aligned} \tag{1}$$

where the linear operators and the fields depend on the ballooning angle θ only, whereas the poloidal wavelength normalized to the ion sound Larmor radius together with the gradients of the plasma species are parameters of the equations, as detailed in [21]. The eigenfunctions of equation (1) can be either drift waves or shear Alfvén waves depending on the amplitude of the fields. Given the following definition

$$\begin{aligned} \Psi &= i\frac{\omega}{c}\delta A_\parallel \\ \Phi &= \frac{1}{qR_0}\partial_\theta \delta\phi \end{aligned} \tag{2}$$

and the ratio $P = |\Psi - \Phi|/|\Phi|$ the solution is nearly electrostatic for $P \approx 1$ while it is a drift-Alfvén wave with nearly shear Alfvén polarization for $P << 1$. The structure of the eigenfunctions of the unstable modes found for T_H=5 keV (Fig 10, α=0.19) are those of the standard electrostatic ITG [30]: the electrostatic potential is even in the ballooning coordinate

θ while the parallel magnetic potential is much smaller and odd. By increasing the temperature of the hydrogen minority (therefore increasing the plasma α) up to T_H=*170* keV (Fig 10, α=*0.38*) the eigenfunctions of the most unstable modes change all over the spectrum: at higher wave numbers ($k_\perp \rho_i \geq 0.6$) the dominant unstable modes are still nearly electrostatic but the parallel magnetic potential is found to have tearing parity, as shown in Fig. 13. At lower wave numbers the unstable modes have nearly shear Alfvén polarization and ITG character (AITG), as shown in Fig. 14; i.e., these are the modes discussed in [21]. The tearing-parity solutions are characterized by small radial scale-length variations which translate into long wavelengths in the ballooning angle and are therefore more difficult to capture numerically. Although in Fig. 13 we show θ ranging between [-20,20], in the calculation we had to vary θ between [-150,150] to allow convergence and prevent strongly oscillating solutions to appear. Microtearing modes arise from a mechanism similar to the violation of the "frozen-in" law in the presence of wave particle interaction as can be seen from the parallel component of Ohm's equation, given by the parallel gradient of Eq. (3):

$$\left(\frac{1}{\tau}+1\right)\left(\delta\varphi-\delta\psi\right)-\frac{T_i}{ne}\sum_s\left\langle J_0\left(k_\perp\rho_s\right)\delta K_s\right\rangle+\left[\left(1-\frac{\omega_{*ni}}{\omega}\right)\left(1-\Gamma_0\right)-\frac{\omega_{*Ti}}{\omega}b_i\left(\Gamma_0-\Gamma_1\right)\right]\delta\psi=0 \qquad (3)$$

Here the notation is that used in [21]. Micro instabilities with tearing parity have been investigated by many authors, e.g. [31,32,33]. In all references the drive of the instability is the gradient of the electron temperature. Here the mode is destabilised by increasing the ion pressure gradient, at constant electron temperature and density gradient. In general the parallel electric field will be non zero and will have a direct contribution from the parallel vector potential, second term on the LHS, and from the non adiabatic part of the distribution functions. The resonant non adiabatic response, needed for the violation of the frozen-in

condition, depends on the spatial scale length, so that Eq. (3) should be further generalized to include finite electron inertia for a correct description of the reconnection process. This is beyond the scope of this work and we limit ourselves to the interpretation of the numerical results obtained from GS2 simulations, based on the physical model discussed in [25]. Unstable micro tearing modes in experimental condition of interest have been predicted in the Mega Ampere Spherical Tokamak, MAST [34] and AUG [35]. Keeping constant the other plasma parameters, as reported in Table I, we have performed the scan in the hydrogen temperature (hence α) for a fixed $k_\perp \rho_i$ chosen such that the unstable mode have micro-tearing parity. We find that the mode is weakly sensitive to a further increase in the ion pressure gradient; however they are fully stabilized for α above a critical threshold value (suggesting the existence of a second stability region in the α space), Fig. 15. A similar scan at smaller $k_\perp \rho_i$ where the AITG are unstable confirms the result of [21], Fig. 16. By increasing the temperature of the hydrogen minority the transition from Alfvénic ITG to microtearing modes occurs at lower values of $k_\perp \rho_i$. It is possible that for sufficiently high energies of the fast-ions the only unstable modes will be drift wave microtearing.

CONCLUSION

The local stability of the ion temperature gradient modes in the presence of a fast-ion minority (hydrogen) has been investigated in a JET hybrid scenario ITB discharge (pulse #59137). The background of this study is the need to model the trigger for the formation of an internal transport barrier (a region where the turbulence is suppressed) in discharges where the magnetic shear is monotonic. Improvement of confinement and transport barrier formation in plasmas with fast ions has already been discussed in previous works, e.g. [19], where it has been attributed to dilution. In this paper we have explored a different mechanism related to the increase of the local pressure-gradient (α) due to the presence of fast ions. The

modification of the pressure-gradient causes a change in the parity of the most unstable modes (marginal stability thresholds [21]) and in the absence of a strong dilution could be an important stabilizing mechanism. In our model, we find that the contribution of the energetic ions to the total plasma pressure in #59137, is enough to locally reach an optimal value of α (just below the threshold of the Alfvénic modes) for which the "electrostatic" ITGs are stable and the Alfvénic modes are still quiescent. This allows the plasma to develop and sustain ion temperature gradients with inverse scale-lengths well above the threshold for unstable electrostatic ITG [24] and trigger the formation of an ion transport barrier. For the plasma parameters of JET #59137 and the gradients of Table I, the ion temperature gradient modes are predicted to be stable for T_H around 170KeV, which is within the range of the temperature of the hydrogen ions accelerated by the ICRH system (above 130KeV). Much higher temperatures would be required for turbulence stabilization in hybrid discharges where the density of the hydrogen minority is lower (e.g. #60933, #62459, where indeed the transport barrier is not observed). We conclude therefore that local stabilization of the ITG modes due to ICRH accelerated hydrogen is a plausible candidate mechanism to explain the appearance of an ion transport barrier in low density plasmas such as JET#59137. It is important to stress here that low density is not in general a requirement for this mechanism to operate. A similar stabilizing effect can be achieved also in high density plasmas in which the population of fast particles is sufficiently high to change the local beta (for instance in the presence of a large α particle population). Although this is a new hypothesis for the onset of the ITB in hybrids scenario plasmas, we have to point out that it is not the only one; within the same scenario the onset was already correlated to the arise of low *m,n* tearing modes at the resonant surface in proximity of the barrier [36]. However the absence of any relevant MHD activity excludes this hypothesis for the cases discussed in this paper.

ACKNOWLEDGMENTS

Useful discussions with Dr F. Zonca are kindly acknowledged.

This work was funded by the UK EPSRC Grant EP/G003955 and the European Communities under the Contract of Association between EURATOM and CCFE and under EFDA. The views and opinions expressed herein do not necessarily reflect those of the European Commission.

The work of one of the authors (Dr. A. Zocco) was funded by the Leverhulme Network for Magnetised Plasma Turbulence and by the Italian Embassy in London.

REFERENCES

[1] "Special Issue on JET," Fusion Sci. and Technol., **53** (2008), No. 4.

[2] K Ikeda, Nucl. Fusion **47** (2007) S1–S17

[3] "Special Issue on DIII-D Tokamak," Fusion Sci. and Technol., **48** (2005), No. 2.

[4] "Special Issue on ASDEX Upgrade, Fusion Sci. and Technol., **44** (2003), No. 3.

[5] "Special Issue on JT-60," Fusion Sci. and Technol., **42 (2002)** No. 2,3.

[6] Challis C.D. Plasma Phys. Control. Fusion **46** (2004) B23.

[7] T. C. Luce, Wade M. R., Ferron J. R., Politzer P. A., and Hyatt A. W., A. C. C. Sips, M. Murakami, Phys. Plasmas **11** (2004) 2627.

[8] A.Isayama, Y. Kamada, T. Ozeki, S. Ide, T.Fujita, T. Oikawa, T. Suzuki, Y. Neyatani, N. Isei, K.Hamamatsu, Y.Ikeda, K.Takahashi, K. Kajiwara and JT-60 Team, Nuclear Fusion, **41** (2001) 761.

[9] J.W. Connor, T. Fukuda, X. Garbet, C. Gormezano, V. Mukhovatov, M. Wakatani, the ITB Database Group, the ITPA Topical Group on Transport and Internal Barrier Physics, et al., Nucl. Fusion **44** (2004) R1-R49

[10] E. Joffrin, A.C.C. Sips, J.F. Artaud, A. Becoulet, L. Bertalot, R. Budny, P. Buratti, P. Belo, C.D. Challis, F. Crisanti, M. de Baar, P. de Vries, C. Gormezano, C. Giroud, O. Gruber, G.T.A. Huysmans, F. Imbeaux, A. Isayama, X. Litaudon, P.J. Lomas, D.C. McDonald, Y.S. Na, S.D. Pinches, A. Staebler, T. Tala, A. Tuccillo, K.-D. Zastrow and JET-EFDA Contributors to the Work Programme, Nucl. Fusion **45** (2005) 626-634

[11] A. Staebler, A.C.C. Sips, M. Brambilla, R. Bilato, R. Dux, O. Gruber, J. Hobirk, L.D. Horton, C.F. Maggi, A. Manini, M. Maraschek, A. Mück, Y.-S. Na, R. Neu, G. Tardini, M.R. Wade and ASDEX Upgrade Team , Nucl. Fusion **45** (2005) 617-62

[12] C.F. Maggi, R.J. Groebner, N. Oyama, R. Sartori, L.D. Horton, A.C.C. Sips,W. Suttrop, T. Leonard, T.C. Luce, M.R. Wade, Y. Kamada, H. Urano,Y. Andrew, C. Giroud, E. Joffrin, E. de la Luna, ASDEX Upgrade Team,DIII-D Team, JT-60U Team, for the Pedestal and Edge Physics,the Steady State Operation Topical Groups of the ITPA,and JET EFDA contributors., Proceedings of the 21st IAEA Fusion Energy Conference, Chengdu, China, Oct. 2006, available at http://www-naweb.iaea.org/napc/physics/fec/fec2006/html/node77.htm#20168

[13] P. Buratti, , B. Alper, S. V. Annibaldi, Plasma Phys. Control. Fusion **48** (2006) 1005-1018.

[14] E Joffrin, R Wolf, B Alper, Yu Baranov, C D Challis, M de Baar, C Giroud, C W Gowers, N C Hawkes, T C Hender, M Marachek, D Mazon, V Parail, A Peeters, K-D Zastrow and contributors to the EFDA-JET Workprogramme, Plasma Phys. Control. Fusion **44** (2002) 1203-1214

[15] G. Tresset, X. Litaudon, D. Moreau, X. Garbet and Contributors to the EFDA-JET Work Programme, Nucl. Fusion **42** (2002) 520–526 [16] K. Crombé, Y. Andrew, M. Brix, C. Giroud, S. Hacquin, N. C. Hawkes, A. Murari, M. F. F. Nave, J. Ongena, V. Parail, G. Van Oost, I. Voitsekhovitch, and K.-D. Zastrow, Phys Rev Lett **95** (2005) 155003-1

[17] G. Cenacchi and A. Taroni (1988) *Rapporto ENEA RT/TIB (88)5*

[18] L. G. Eriksson, T. Hellsten, U. Willen, Nuclear Fusion **33** (1993) 1037

[19] G. Tardini, J. Hobirk, V.G. Igochine, C.F. Maggi, P. Martin, D. McCune, A.G. Peeters, A.C.C. Sips, A. Stäbler, J. Stober and the ASDEX Upgrade Team, Nucl. Fusion **47** (2007) 280–287

[20] J. Y. Kim, W. Horton and J. Q. Dong, Phys. Fluids B **5**, 4030 (1993)

[21] F. Zonca F., L.Chen , J. Q. Dong, and R. A. Santoro *et al*, Phys. Plasmas, **6** (1999) 1917

[22] F. Zonca, L. Chen and R.A. Santoro, Plasma Phys. Control. Fusion **38** (1996) 2011

[23] F. Zonca, L. Chen, R.A. Santoro and J.Q. Dong, Plasma Phys. Control. Fusion **40** (1998) 2009

[24] P. Mantica, D. Strintzi, T. Tala, C. Giroud, T. Johnson, H. Leggate, E. Lerche, T. Loarer, A. G. Peeters, A. Salmi, S. Sharapov, D. Van Eester, P. C. de Vries, L. Zabeo, and K.-D. Zastrow, Phys. Rev. Lett. **102** (2009), 175002

[25] M. Kotschenreuther , G. Rewoldt , and M. W. Tang, Comp. Phys. Com. **88** (1995) 128

[26] M.Romanelli, G. Regnoli, C. Bourdelle, Phys. Plasmas **14** (2007) 082305

[27] F. Crisanti, A. Becoulet, P. Buratti, E. Giovannozzi, C. Gormezano, E. Joffrin, A. Sips, C. Bourdelle, A. Cardinali, C. Challis, N. Hawkes, J. Hobirk, X. Litaudon, G. Regnoli, M. Romanelli, A. Thyagaraja, A. Tuccillo, and JET EFDA Contributors, Proceedings of the 21st IAEA Fusion Energy Conference 16-21 October (2007) Chengdu

[28] G. Vlad, S. Briguglio, G. Fogaccia and F. Zonca, Plasma Phys. Contr. Fusion **46** (2004) S81

[29] C. Bourdelle, G.T. Hoang, X. Litaudon, C.M. Roach and T. Tala for the ITPA Topical Group on Transport and ITB Physics, and the International ITB Database Working Group, Nucl. Fusion **45** (2005) 110–130

[30] F. Romanelli and F. Zonca, Phys. Fluids B **5** (1993) 4081

[31] B. Coppi, J.W.K. Mark, L. Sugiyama, G. Bertin, Phys. Rev. Lett. **42** (1979) 1058 - 1061

[32] J.F. Drake, N. T. Gladd, C. S. Liu and C. L. Chang, Phys. Rev. Letters **44** (1980)

[33] J.W. Connor, S.C. Cowley and R. J. Hastie, Plasma Phys. Contr Fusion, **32** (1990)

[34] D.J. Applegate, C.M. Roach, S.C. Cowley, W.D. Dorland, Joiner N , R.J. Akers, N.J. Conway, A.R. Field, A. Patel , M. Valovic , M.J. Walsh, Phys. Plasmas, **11** (2004) 5085

[35] L. Vermare, C. Angioni, P. Bottino, A. G. Peeters, Journal of Physics: Conference Series **123** (2008) 012040

[36] E. Joffrin et al., Nucl. Fusion **42** 235-242 (2002)

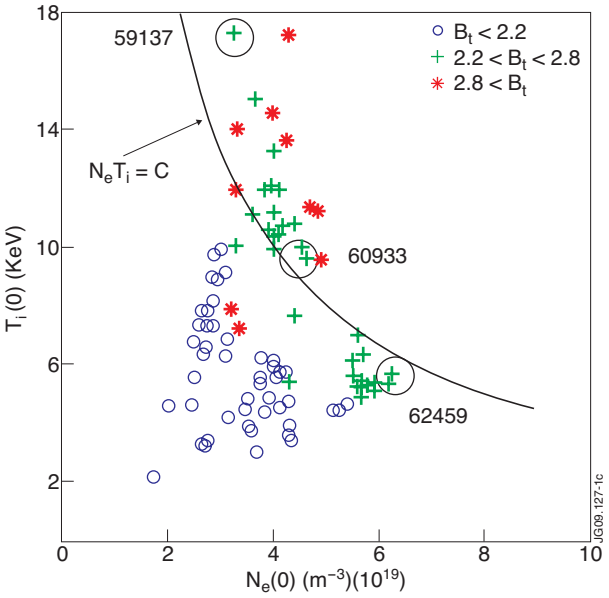

Figure 1: Central ion temperature $T_i(0)$ versus central electron density $N_e(0)$ of shots in the JET hybrid-scenario database with same input power. The data are divided in three ranges of toroidal field B_T (T). Three discharges similar in all operational parameter, except for the density, are shown for comparison. The line identifies points of the plane with constant $N_e(0)$ $T_i(0)$.

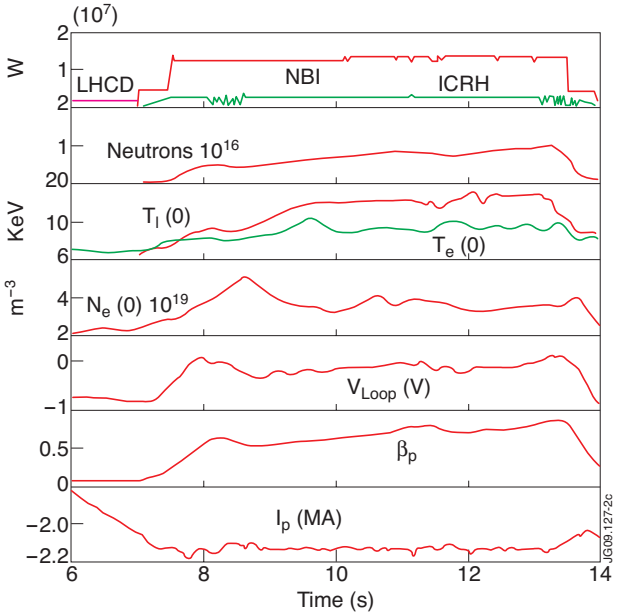

Figure 2: Pulse No: 59137 time traces of heating and main plasma parameters. The sign of the plasma current and loop voltage shown is conventionally used in JET experiments (the actual value of the plasma current and loop voltage is obtained by multiplying the signal by -1).

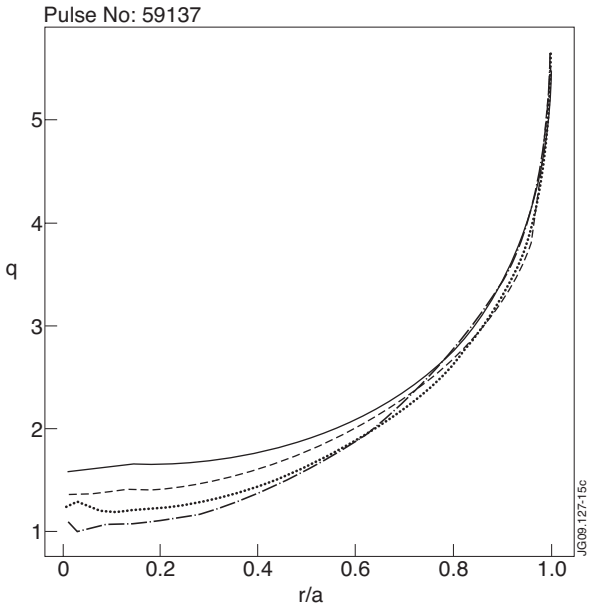

Figure 3: Radial profiles of the safety factor q at four different times for Pulse No: 59137. Full line (largest central value) t=8.4s; dashed line t=8.9s; dotted line t=10.1s; dashed dotted line (smallest central value) t=11.9s

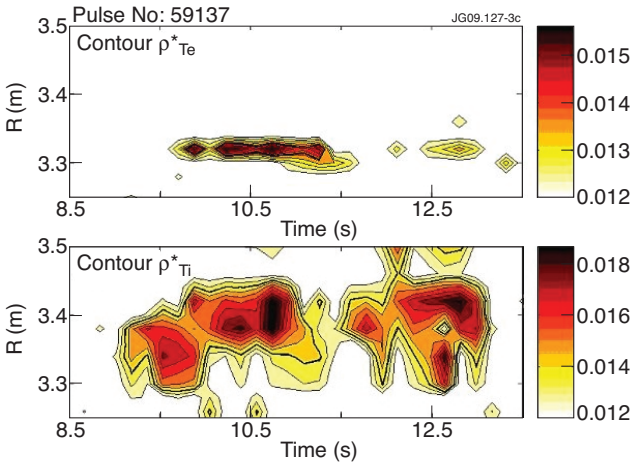

Figure 4: Pulse No: 59137. Normalized electrons (upper chart) and ions (lower chart) Larmor radius equi-contour versus time. R=3.3m corresponds to r/a=0.33 and R=3.5m to r/a=0.55. The ITB forms around t=9.0s.

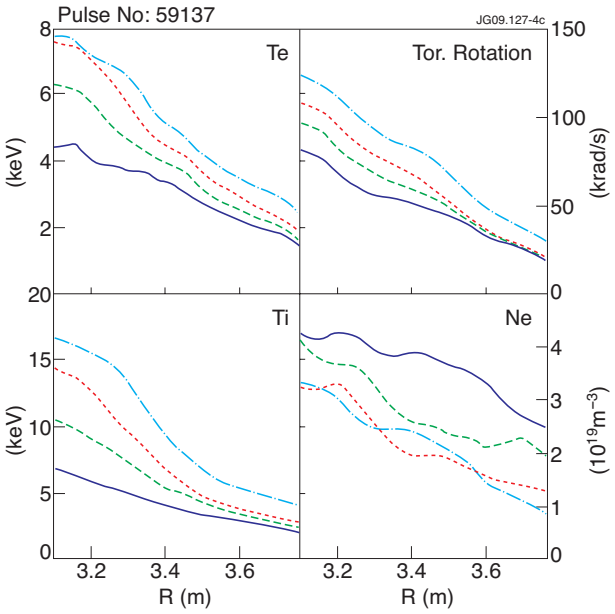

Figure 5: Radial profiles of the electron and ion temperature (T_e, T_i), of the electron density (N_e) and of the toroidal rotation at four times for the discharge No: 59137. Solid line t=8.4s; dashed t=8.9s; dots t=10.1s; semi dashed t=11.9s

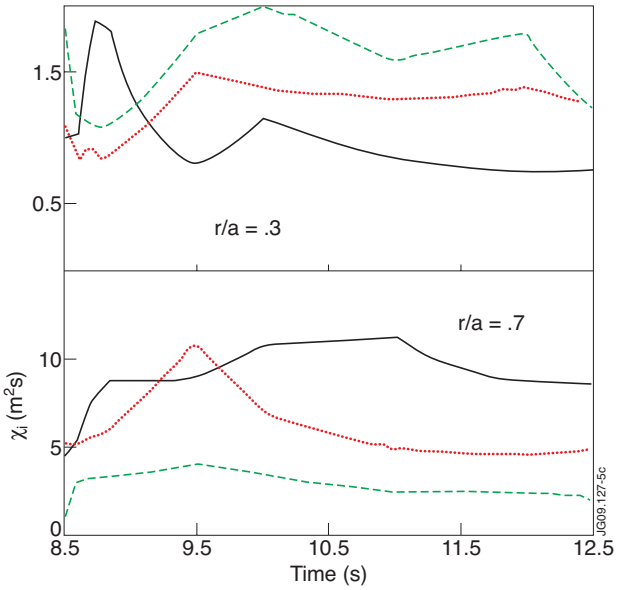

Figure 6: Time traces of heat conductivities at two different radial positions: r/a=0.3, R=3.3m upper box and r/a=0.7, R=3.7m lower box. Pulse No's: 59137 (full line, line average density $n_e=2\times10^{19}$ m^{-3}), 60933 (dotted line, $n_e=3\times10^{19}$ m^{-3}), 62459 (dashed line, $n_e=5.5\times10^{19}$ m^{-3}).

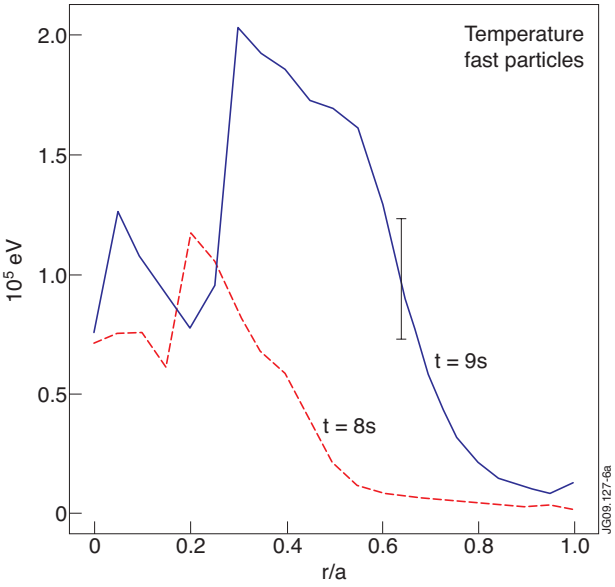

Figure 7: PION, energetic hydrogen temperature profiles Pulse No: 59137 @: t=8.0s (before the barrier formation), t=9.0s (at the barrier formation). The estimated error (30%) of the fast ion temperature is shown around the maximum of the power deposition profile.

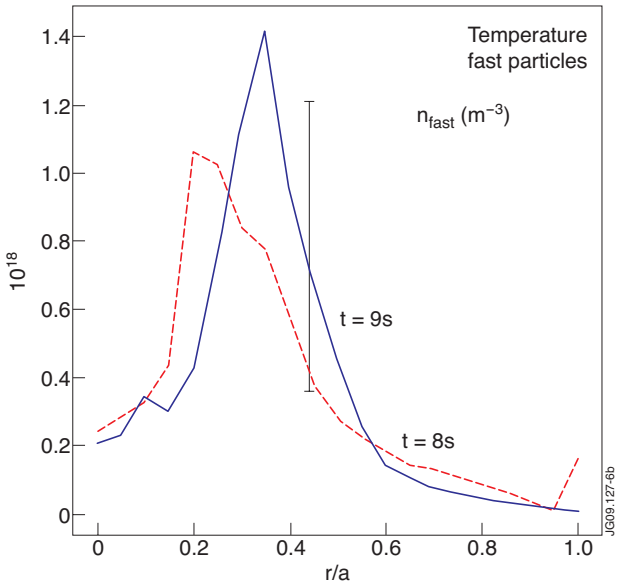

Figure 8: PION, energetic hydrogen density profiles Pulse No: 59137 @: t=8.0s (before the barrier formation), t=9.0s (at the barrier formation). A relative error of 50% is estimated for the fast ion density.

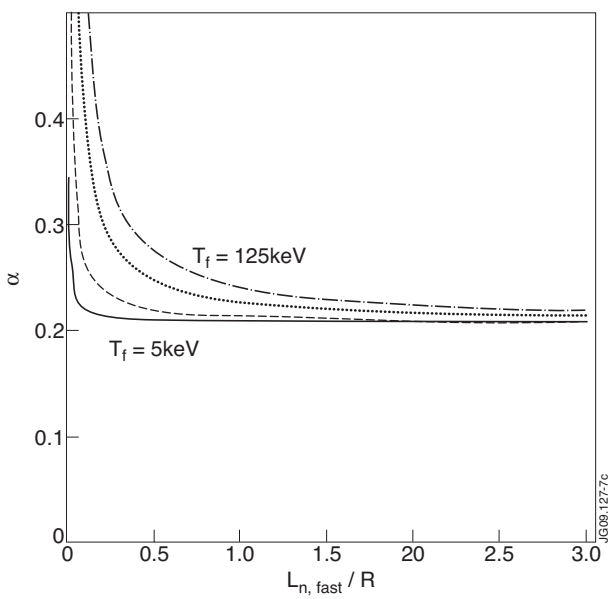

Figure 9: Dependence of α on the normalized inverse density gradient scale-length fast fast fast $L_{n,fast} = n_{fast} / \nabla n_{fast}$, for four different values of the fast ion temperature (between 5 keaV and 125 keV). By varying the temperature of the minority within the same range a wider range of α can be scanned at $L_{n,fast}/R$, around 1 and below.

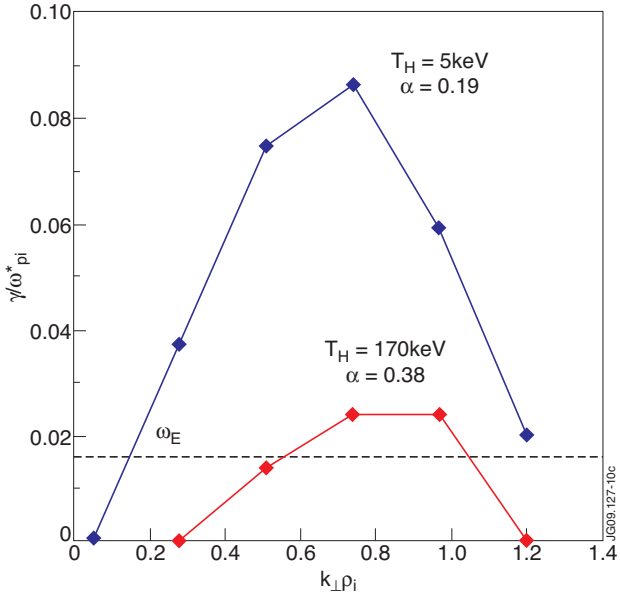

Figure 10: Spectrum of the unstable (electromagnetic) modes with warm (thermal) and hot (energetic) minority hydrogen. Although zonal flows are not included in the calculation of the growth rate, the $\omega_{E\times B}$ rate is also plotted as indicative reference value. The most unstable modes appear in the range $k_\perp\rho\in$ [0.5,1.0]

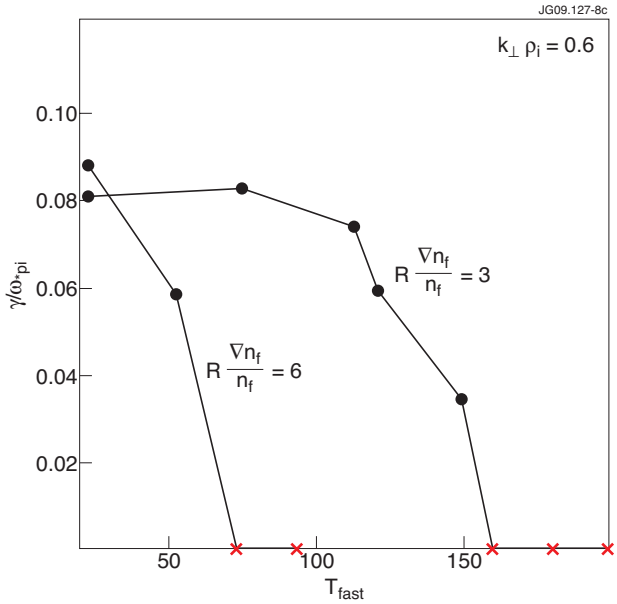

Figure 11: Scaling of the normalized growth rate of the most unstable (electrostatic) modes ($k_\perp\rho$=0.6) versus the temperature of the hydrogen minority normalized to the deuterium temperature, for two different values of its density gradient, plasma parameters from Table 1.

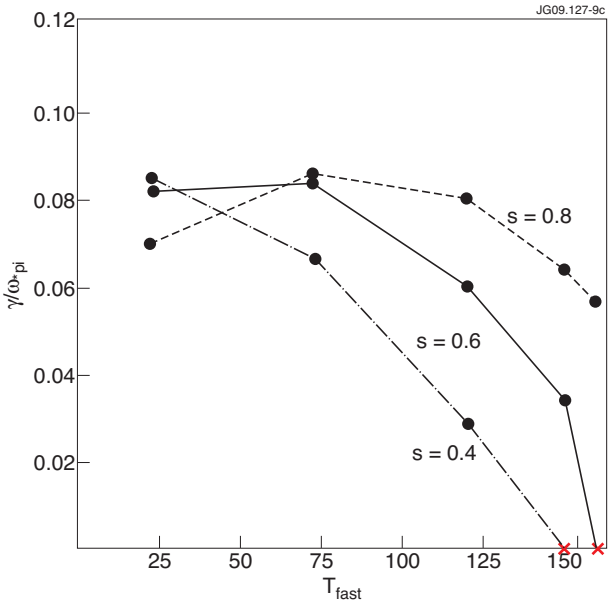

Figure 12: Scaling of the normalized growth rate of one of the most unstable (electrostatic) modes ($k_\perp\rho$=0.6) versus the temperature of the hydrogen minority normalized to the deuterium temperature for three different values of the magnetic shear (s=0.4 lower dashed line, s=0.6 full line, s=0.8 upper dashed line) and for R/ $L_{n,fast}$ = 3.

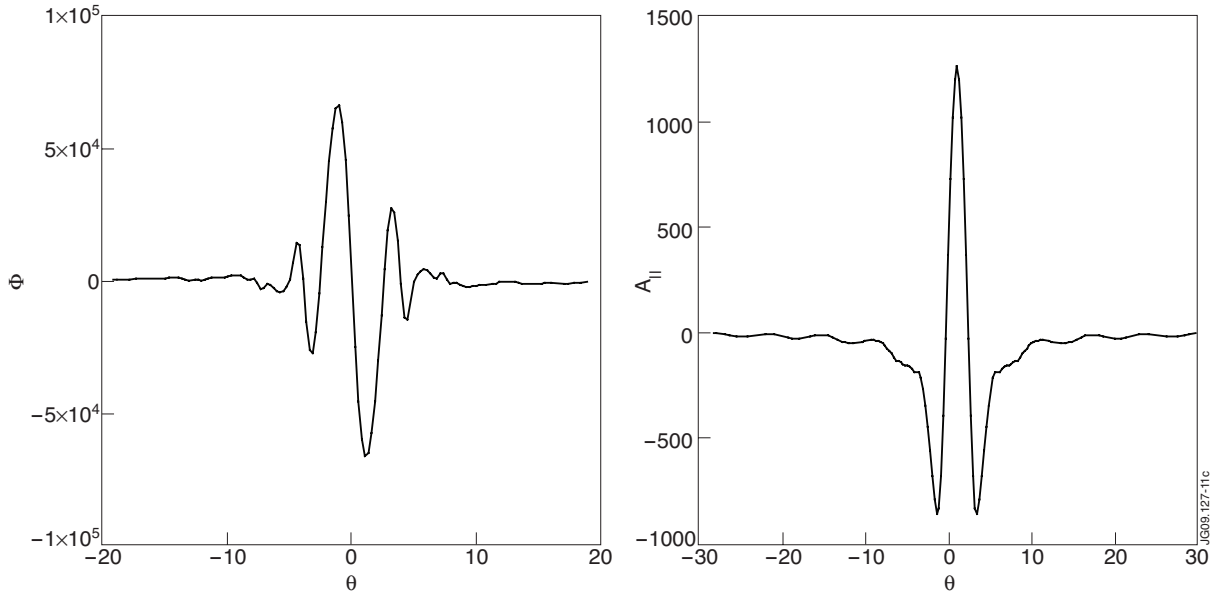

Figure 13: Unstable mode at $k_\perp \rho_i \geq 0.6$ (see spectrum of figure 10, α=0.38). Electrostatic potential and parallel magnetic potential versus ballooning angle.

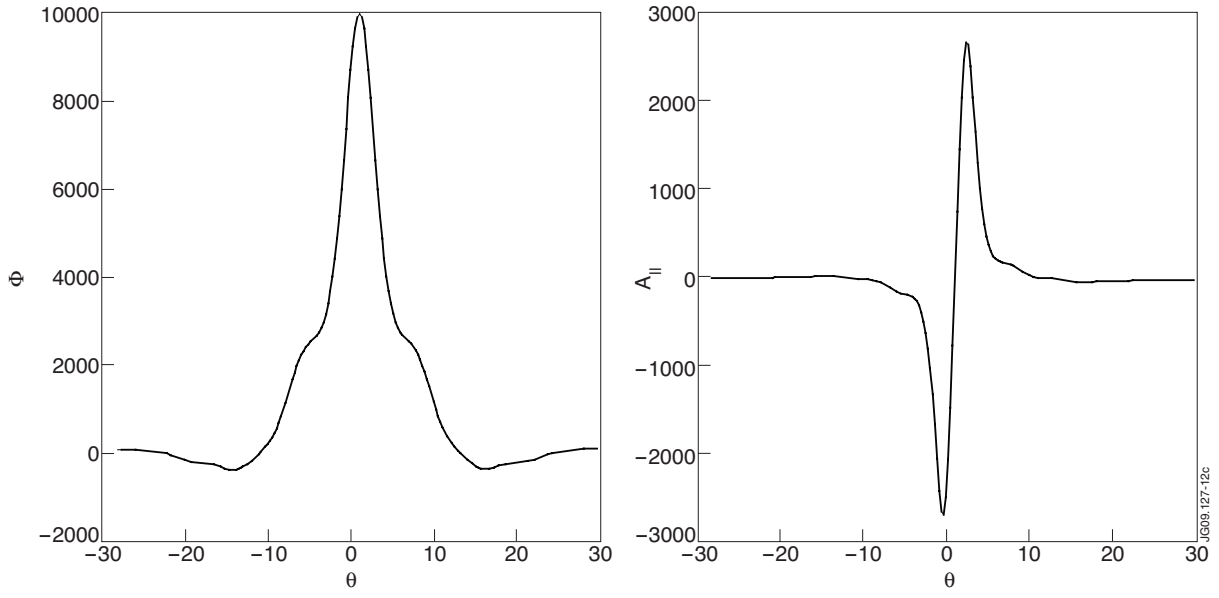

Figure 14: Unstable mode at $k_\perp \rho_i \geq 0.6$ (see spectrum of figure 10, α=0.38). Electrostatic potential and parallel magnetic potential versus ballooning angle.

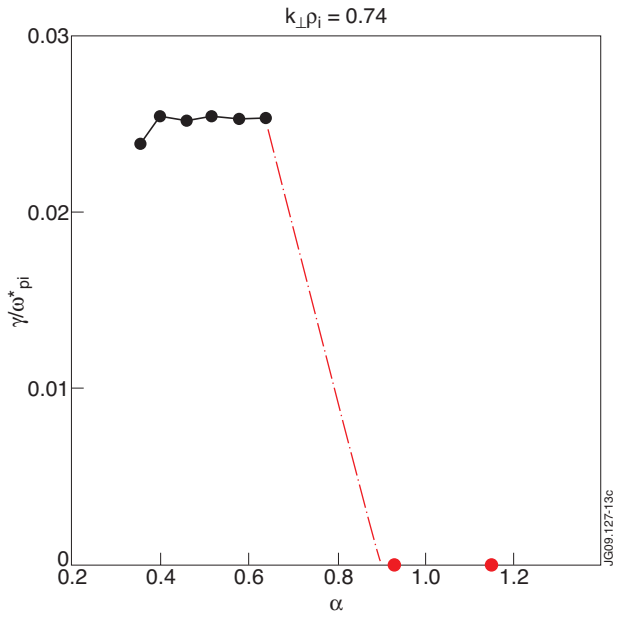

Figure 15: Normalized linear growth rate of tearing parity modes versus α. The modes are found stable for α exceeding 0.8 (see the two points on the x axis).

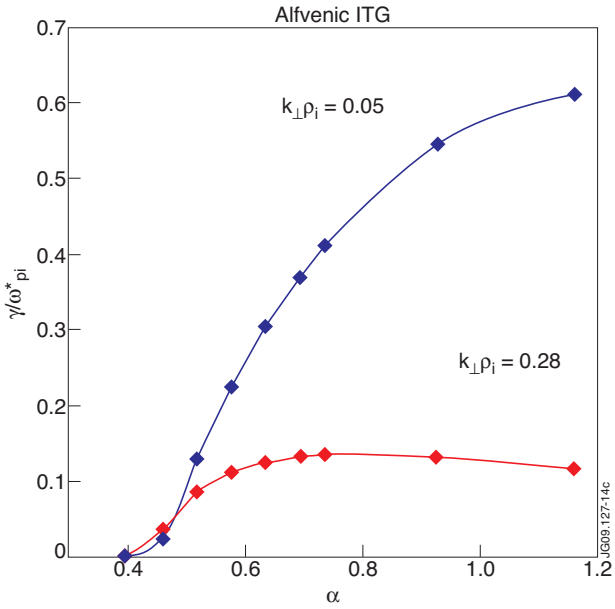

Figure 16: Normalized linear growth rate of AITG modes versus α. The growth rate is found to saturate at large values of α.

Species	*n ($10^{19}m^{-3}$)*	*R∇n/n*	*R∇T/T*	*T (keV)*
D^2	*1.01*	*4.16*	*11.47*	*5*
e^-	*1.94*	*2.72*	*3.59*	*3.4*
C^{6+}	*0.13*	*0.69*	*5.23*	*5*
H^1	*0.15*	*4.16*	*0*	*5 - 800*

Table I: Summary of normalized gradient lengths, temperatures and concentrations of plasma species in JET Pulse No: 59137, at r/a=0.5 and t=10s, used in the GS2 analysis.